

# On Surface Area and Length Preserving Flows of Closed Curves on a Given Surface



Miroslav Kolář, Michal Beneš, and Daniel Ševčovič

**Abstract** In this paper we investigate two non-local geometric geodesic curvature driven flows of closed curves preserving either their enclosed surface area or their total length on a given two-dimensional surface. The method is based on projection of evolved curves on a surface to the underlying plane. For such a projected flow we construct the normal velocity and the external nonlocal force. The evolving family of curves is parametrized by a solution to the fully nonlinear parabolic equation for which we derive a flowing finite volume approximation numerical scheme. Finally, we present various computational examples of evolution of the surface area and length preserving flows of surface curves. We furthermore analyse the experimental order of convergence. It turns out that the numerical scheme is of the second order of convergence.

## 1 Introduction

In this article we discuss a motion of closed and nonselfintersecting curves  $\mathcal{G}_t$ ,  $t \geq 0$ , on a given two dimensional surface  $\mathcal{M} \subset \mathbb{R}^3$ . We suppose that the surface  $\mathcal{M}$  is represented by the graph of a given smooth function  $\varphi : \mathbb{R}^2 \rightarrow \mathbb{R}$  and the curve  $\mathcal{G}_t$  is evolved in the outer normal direction by the following nonlocal geometric evolution

---

M. Kolář (✉) · M. Beneš

Department of Mathematics, Faculty of Nuclear Sciences and Physical Engineering,  
Czech Technical University in Prague, Prague, Czech Republic  
e-mail: [kolarmir@fjfi.cvut.cz](mailto:kolarmir@fjfi.cvut.cz); [michal.benes@fjfi.cvut.cz](mailto:michal.benes@fjfi.cvut.cz)

D. Ševčovič

Department of Applied Mathematics and Statistics, Faculty of Mathematics, Physics and  
Informatics, Comenius University, Mlynská Dolina, Bratislava, Slovakia  
e-mail: [sevcovic@fmph.uniba.sk](mailto:sevcovic@fmph.uniba.sk)

© Springer Nature Switzerland AG 2019

F. A. Radu et al. (eds.), *Numerical Mathematics and Advanced Applications  
ENUMATH 2017*, Lecture Notes in Computational Science and Engineering 126,  
[https://doi.org/10.1007/978-3-319-96415-7\\_24](https://doi.org/10.1007/978-3-319-96415-7_24)

279

equation:

$$\mathcal{V}_{\mathcal{G}} = -\mathcal{K}_{\mathcal{G}} + \mathcal{F}, \quad (1)$$

where  $\mathcal{G}_t|_{t=0} = \mathcal{G}_{ini} \subset \mathcal{M}$  is the initial condition—a  $C^1$  smooth Jordan curve,  $\mathcal{V}_{\mathcal{G}}$  is the normal velocity,  $\mathcal{K}_{\mathcal{G}}$  is the geodesic curvature of the curve  $\mathcal{G}_t$ , and  $\mathcal{F}$  is the nonlocal force term. We present results of the surface area preserving geodesic curvature flow with the force  $\mathcal{F}_A$ , and the length preserving geodesic curvature flow with the force  $\mathcal{F}_L$ . The surface area preserving flow has been analysed in the recent paper [1]. In this paper we furthermore investigate the length preserving flow of surface curves. We compare both types of preserving flows.

Recall that the length  $L(\mathcal{G}_t)$  and the enclosed surface area  $A(\mathcal{G}_t)$  of a surface closed curve  $\mathcal{G}_t$  satisfy the following identities:

$$\frac{d}{dt}L(\mathcal{G}_t) = \int_{\mathcal{G}_t} \mathcal{K}_{\mathcal{G}} \mathcal{V}_{\mathcal{G}} d\mathcal{S}, \quad \frac{d}{dt}A(\mathcal{G}_t) = \int_{\mathcal{G}_t} \mathcal{V}_{\mathcal{G}} d\mathcal{S},$$

(see e.g. [1]). With help of these identities the nonlocal forces given by

$$\mathcal{F}_A = \frac{1}{L(\mathcal{G}_t)} \int_{\mathcal{G}_t} \mathcal{K}_{\mathcal{G}} d\mathcal{S}, \quad \mathcal{F}_L = \frac{\int_{\mathcal{G}_t} \mathcal{K}_{\mathcal{G}}^2 d\mathcal{S}}{\int_{\mathcal{G}_t} \mathcal{K}_{\mathcal{G}} d\mathcal{S}},$$

represent the surface area and length preserving flows, respectively.

The constrained motion driven by (1) is a generalization of the geometric motion in the plane, which is broadly discussed in the literature (see, e.g., [2–6] for the area-preserving flow or, e.g., [7] for the length-preserving flow). In general, the physical context of moving interfaces driven by the curvature is also discussed in [8, 9] within the context of the Allen-Cahn equation [10, 11] or within the context of the recrystallization effects (see [12]).

## 2 Parametric Description and Projection to the Plane

In accordance with [1, 13], the geometric motion law (1) is treated by means of the vertical projection  $\Gamma_t$  of a surface curve  $\mathcal{G}_t$  to the plane, i.e.,  $\mathcal{G}_t = \{(\mathbf{X}, \varphi(\mathbf{X})^T : \mathbf{X} \in \Gamma_t)\}$ . Here  $\Gamma_t$  denotes the time-dependent closed projected planar curve moving in the normal direction (see Fig. 1). Then,  $\Gamma_t$  is described by the position vector  $\mathbf{X} = \mathbf{X}(u, t)$ ,  $u \in [0, 1]$ , where  $u$  is a parameter from a fixed interval, and  $\mathbf{X}$  is required to be 1-periodic in  $u$ .

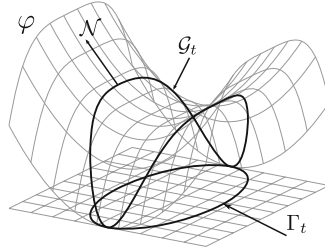


**Fig. 1** An example of a curve  $\mathcal{G}_t$  with an outer normal vector  $\mathcal{N}$  on a given surface  $\mathcal{M} = \text{graph}(\varphi)$  and its projection  $\Gamma_t$  to the underlying plane  $\mathbb{R}^2$  (see [1])

Similarly to [1, 14, 15], one can derive a system of governing equations for the parametrization  $\mathbf{X}(u, t)$  of the curve  $\Gamma_t$ , provided that  $\mathcal{G}_t$  evolves on the surface  $\mathcal{M}$  in the normal direction by the velocity  $\mathcal{V}_{\mathcal{G}}$ . Then  $\mathcal{V}_{\mathcal{G}} = \left( \frac{1+|\nabla\varphi|^2}{1+(\nabla\varphi \cdot \mathbf{t}_{\Gamma})^2} \right)^{\frac{1}{2}} v_{\Gamma}$  where  $v_{\Gamma}$  is the normal velocity of the projected curve  $\Gamma_t$  (see [14]). We assume the parametrization  $\mathbf{X}$  is oriented counter-clockwise, and that the periodic boundary conditions for  $\mathbf{X}$  at  $u = 0$  and  $u = 1$  are imposed, i.e.,  $\mathbf{X}|_{u=0} = \mathbf{X}|_{u=1}$  and  $\partial_u \mathbf{X}|_{u=0} = \partial_u \mathbf{X}|_{u=1}$ . Then, the unit tangential vector  $\mathbf{t}_{\Gamma}$ , the outer unit normal vector  $\mathbf{n}_{\Gamma}$ , and the curvature  $\kappa_{\Gamma}$  of  $\Gamma_t$  are expressed in terms of  $\mathbf{X}$  as the following

$$\mathbf{t}_{\Gamma} = \frac{\partial_u \mathbf{X}}{|\partial_u \mathbf{X}|}, \quad \mathbf{n}_{\Gamma} = \frac{\partial_u \mathbf{X}^{\perp}}{|\partial_u \mathbf{X}|}, \quad \kappa_{\Gamma} = -\frac{1}{|\partial_u \mathbf{X}|} \frac{\partial}{\partial u} \left( \frac{\partial_u \mathbf{X}}{|\partial_u \mathbf{X}|} \right) \cdot \mathbf{n}_{\Gamma}.$$

Here  $\mathbf{a} \cdot \mathbf{b}$  denotes the Euclidean inner product of vectors  $\mathbf{a}$  and  $\mathbf{b}$ . For a curve  $\mathcal{G}_t$  on the surface  $\mathcal{M}$ , its geodesic curvature can be expressed in terms of properties of  $\Gamma_t$  as follows (see [1, 14]):

$$\mathcal{K}_{\mathcal{G}} = \frac{(1 + |\nabla\varphi|^2)^{1/2} \kappa_{\Gamma} - \frac{\mathbf{t}_{\Gamma}^T \nabla^2 \varphi \mathbf{t}_{\Gamma}}{(1+|\nabla\varphi|^2)^{1/2}} (\nabla\varphi \cdot \mathbf{n}_{\Gamma})}{(1 + (\nabla\varphi \cdot \mathbf{t}_{\Gamma})^2)^{3/2}}.$$

Having this geometrical framework, one can construct a geometric equation for the normal velocity  $v_{\Gamma}$  of  $\Gamma_t$  as  $v_{\Gamma} = \beta(\mathbf{X}, \mathbf{n}_{\Gamma}, \kappa_{\Gamma})$ , where  $\beta$  is the normal component of the velocity of the planar curve  $\Gamma_t$ , i.e.,  $\beta = \partial_t \mathbf{X} \cdot \mathbf{n}_{\Gamma}$ . For technical details on the derivation of the following system of equations, we refer the reader to, e.g., [1]. The curve  $\mathcal{G}_t$  evolves according to the motion law (1) provided the parametrization  $\mathbf{X}(u, t)$  of the projected curve  $\Gamma_t$  satisfies the following system of nonlinear parabolic equations:

$$\partial_t \mathbf{X} = a \frac{1}{|\partial_u \mathbf{X}|} \frac{\partial}{\partial u} \left( \frac{\partial_u \mathbf{X}}{|\partial_u \mathbf{X}|} \right) + (b + c\mathcal{F}) \frac{\partial_u \mathbf{X}^{\perp}}{|\partial_u \mathbf{X}|}, \tag{2}$$

subject to the initial condition  $\mathbf{X}|_{t=0} = \mathbf{X}_{ini}$ , and

$$a = \frac{1}{1 + (\nabla\varphi \cdot \mathbf{t}_\Gamma)^2}, \quad b = \frac{\mathbf{t}_\Gamma^T \nabla^2\varphi \mathbf{t}_\Gamma (\nabla\varphi \cdot \mathbf{n}_\Gamma)}{(1 + (\nabla\varphi \cdot \mathbf{t}_\Gamma)^2)(1 + |\nabla\varphi|^2)},$$

$$c = \left( \frac{1 + (\nabla\varphi \cdot \mathbf{t}_\Gamma)^2}{1 + |\nabla\varphi|^2} \right)^{\frac{1}{2}}.$$

### 3 Numerical Solution

In our approach the projected planar curve  $\Gamma_t$  is replaced by a piece-wise linear curve, and for spatial discretization, the technique of flowing finite volume method is used. The principle of the method can be found in, e.g., [1, 2, 16]. The method was successfully applied in, e.g., dislocation dynamics [17], image processing [18] or computational geometry [2]. The method is based on positioning of discrete nodes  $\mathbf{X}_i = \mathbf{X}(u_i, t)$  for  $i = 0, 1, \dots, M$ , along the curve  $\Gamma_t$ . Then, linear segments connecting the neighboring nodes represent the finite volumes. We denote the length of a finite volume as  $d_i = |\mathbf{X}_i - \mathbf{X}_{i-1}|$  for  $i = 1, 2, \dots, M$ , where  $\mathbf{X}_0 = \mathbf{X}_M$ . Additionally, we denote  $\varphi_i = \varphi(\mathbf{X}_i)$ , and  $\mathcal{D}_i = |(\mathbf{X}_i, \varphi_i) - (\mathbf{X}_{i-1}, \varphi_{i-1})|$  as the length of the segment of the discretized curve  $\mathcal{G}_t$ . The approximation of the unit tangent and normal vectors is as follows:

$$\mathbf{t}_j = \frac{\mathbf{X}_{j+1} - \mathbf{X}_{j-1}}{d_{j+1} + d_j}, \quad \mathbf{n}_j = \frac{\mathbf{X}_{j+1}^\perp - \mathbf{X}_{j-1}^\perp}{d_{j+1} + d_j},$$

and the discrete geodesic curvature is calculated as:

$$\mathcal{K}_i = \frac{(1 + |\nabla\varphi_i|^2)^{1/2} \kappa_i - \frac{\mathbf{t}_i^T \nabla^2\varphi_i \mathbf{t}_i}{(1 + |\nabla\varphi_i|^2)^{1/2}} (\nabla\varphi_i \cdot \mathbf{n}_i)}{(1 + (\nabla\varphi_i \cdot \mathbf{t}_i)^2)^{3/2}}. \quad (3)$$

Finally, the semidiscrete scheme for solving (2) then reads as follows:

$$\frac{d\mathbf{X}_i}{dt} \frac{d_{i+1} + d_i}{2} = a_i \left( \frac{\mathbf{X}_{i+1} - \mathbf{X}_i}{d_{i+1}} - \frac{\mathbf{X}_i - \mathbf{X}_{i-1}}{d_i} \right) + (b_i + c_i \mathcal{F}) \frac{(\mathbf{X}_{i+1}^\perp - \mathbf{X}_{i-1}^\perp)}{2}, \quad (4)$$

$$a_j = \frac{1}{1 + (\nabla\varphi_j \cdot \mathbf{t}_j)^2}, \quad b_j = \frac{\mathbf{t}_j^T \nabla^2\varphi_j \mathbf{t}_j (\nabla\varphi_j \cdot \mathbf{n}_j)}{(1 + (\nabla\varphi_j \cdot \mathbf{t}_j)^2)(1 + |\nabla\varphi_j|^2)}, \quad (5)$$

$$c_j = \left( \frac{1 + (\nabla\varphi_j \cdot \mathbf{t}_j)^2}{1 + |\nabla\varphi_j|^2} \right)^{\frac{1}{2}}, \quad (6)$$

satisfying the initial condition  $\mathbf{X}_i(0) = \mathbf{X}_{ini}(u_i)$  for  $i = 1, 2, \dots, M$  and  $\mathcal{F} = \mathcal{F}_A$  in the case of the surface area-preserving flow and  $\mathcal{F} = \mathcal{F}_L$  in the case of length-preserving flow (see [1]). The terms  $\mathcal{F}_A$  and  $\mathcal{F}_L$  are given by

$$\mathcal{F}_A = \frac{1}{\sum_{j=1}^M \mathcal{D}_j} \sum_{j=1}^M \mathcal{K}_j \frac{\mathcal{D}_{j+1} + \mathcal{D}_j}{2}, \quad \mathcal{F}_L = \frac{\sum_{j=1}^M \mathcal{K}_j^2 \frac{\mathcal{D}_{j+1} + \mathcal{D}_j}{2}}{\sum_{j=1}^M \mathcal{K}_j \frac{\mathcal{D}_{j+1} + \mathcal{D}_j}{2}}.$$

### 4 Computational Experiments

We present our qualitative and quantitative results of computational studies for the surface area-preserving and length-preserving flows of closed curves evolving on a surface driven by (1). Both problems are treated by the numerical scheme (4)–(6) for parametric equation (2). In the following examples we demonstrate how solutions of (1) evolve in time and converges towards stationary curves.

For the quantitative analysis, we measure the experimental orders of convergence (EOC) for our numerical scheme. We perform evaluation of EOC in such a way that the conserved quantities—the surface area  $A(\mathcal{G}_t)$  enclosed by the curve  $\mathcal{G}_t$  and the length  $L(\mathcal{G}_t)$  of the curve  $\mathcal{G}_t$  serve as testing parameters for computations of EOCs. In the case of the surface area-preserving flow, we evaluate differences given by the area at the initial time  $A(\mathcal{G}_{ini})$ , and the areas  $A(\mathcal{G}_{T_i})$  at given data output times  $T_i, i = 1, \dots, N$ , i.e.,  $e_i = |A(\mathcal{G}_{T_i}) - A(\mathcal{G}_{ini})|$ . For the length-preserving flow, the differences between the initial length  $L(\mathcal{G}_{ini})$  and lengths  $L(\mathcal{G}_{T_i})$  were measured for same time levels  $T_i$ , i.e.,  $e_i = |L(\mathcal{G}_{ini}) - L(\mathcal{G}_{T_i})|$ . Considering a mesh with  $M$  segments, the following maximum and discrete  $L_1$  (with time stepping  $\Delta t_k$ ) norms of errors depending on the number of finite volumes  $M$  are evaluated as follows:

$$error_{max}(M) = \max_{k=1,2,\dots,N} e_k, \quad error_{L_1}(M) = \frac{1}{T_N} \sum_{k=1}^N e_k.$$

The order of convergence of the scheme (4)–(6) between two meshes with  $M_1$  and  $M_2$  volumes is estimated as

$$EOC = \frac{\ln\left(\frac{error_I(M_1)}{error_I(M_2)}\right)}{\ln\left(\frac{M_2}{M_1}\right)}, \quad I \in \{\max, L_1\}.$$

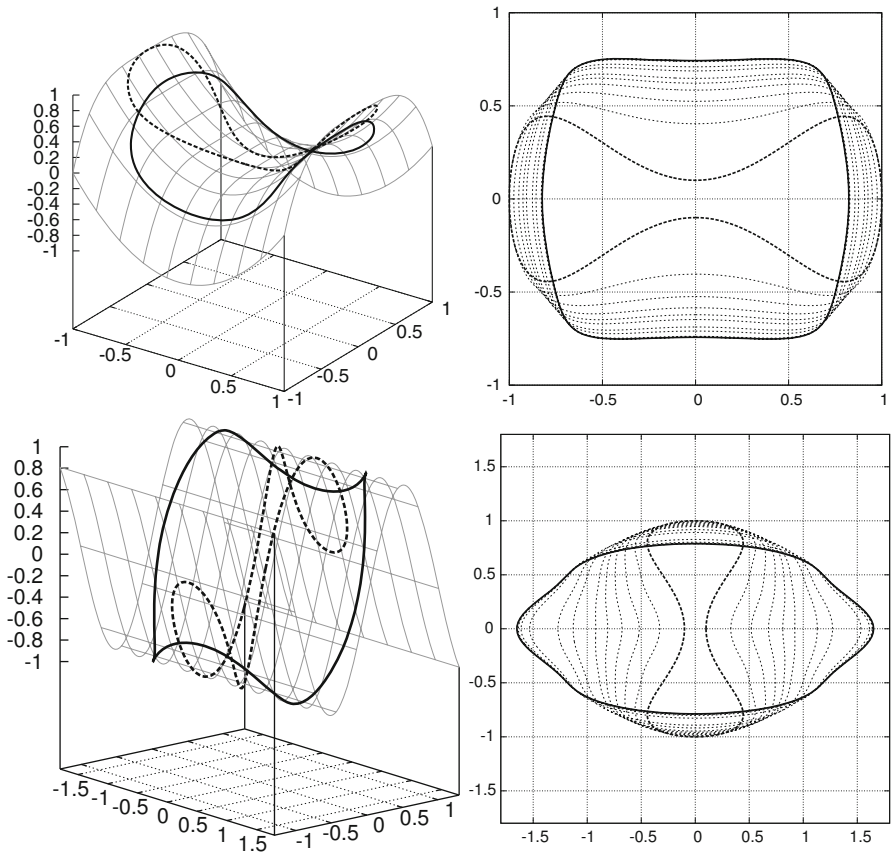


**Fig. 2** Examples of the length-preserving flow of the surface curve  $\mathcal{G}_t$  on two different surfaces  $\mathcal{M}$  and its projection  $\Gamma_t$  to plane. The EOCs are shown in Table 1

In the following computational experiments shown in Figs. 2 and 3, we investigate the length and surface area preserving flows driven by (1) on the surface  $\mathcal{M}$  given by a graph of the function  $\varphi(x, y) = x^2 - y^4$  (top) and  $\varphi(x, y) = \sin(\pi y)$  (bottom). In both sets of examples, we chose a dumbbell shaped initial curve and its rotation by  $90^\circ$  given by the parametrization  $\mathbf{X}_{ini}(u) = (\sin(2\pi u), -(\sin(2\pi u))^2 + 0.1) \cos(2\pi u)$ ,  $u \in [0, 1]$ . We also computed EOCs for the length (Table 1) and surface area preserving flow (Table 2). In both experiments the EOC is approximately 2 which indicates that the numerical scheme is of the second order of experimental convergence.

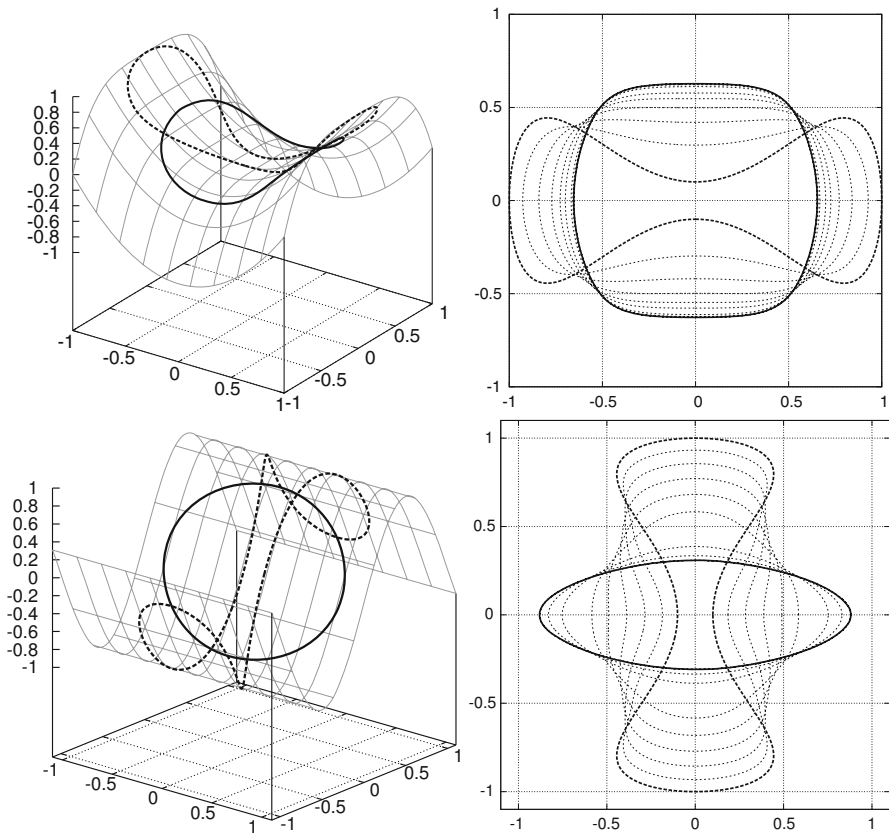


**Fig. 3** Examples of the surface area-preserving flow of the surface curve  $\mathcal{G}_t$  on two different surfaces  $\mathcal{M}$  and its projection  $\Gamma_t$  to plane. The EOCs are shown in Table 2

**Table 1** EOCs for the length-preserving flow depicted in Fig. 2

$M$	$error_{max}$	EOC	$error_{L_1}$	EOC
<i>The surface <math>\mathcal{M}</math> with <math>\varphi(x, y) = x^2 - y^4</math></i>				
100	$2.45246 \cdot 10^{-3}$	–	$2.45246 \cdot 10^{-3}$	–
200	$6.06811 \cdot 10^{-4}$	2.0149	$5.84099 \cdot 10^{-4}$	2.0143
300	$2.69402 \cdot 10^{-4}$	2.0026	$2.59340 \cdot 10^{-4}$	2.0024
400	$1.51633 \cdot 10^{-4}$	1.9978	$1.45975 \cdot 10^{-4}$	1.9977
500	$9.71800 \cdot 10^{-5}$	1.9937	$9.35550 \cdot 10^{-5}$	1.9936
<i>The surface <math>\mathcal{M}</math> with <math>\varphi(x, y) = \sin(\pi y)</math></i>				
100	$4.53052 \cdot 10^{-3}$	–	$4.30824 \cdot 10^{-3}$	–
200	$1.15305 \cdot 10^{-3}$	1.9742	$1.09608 \cdot 10^{-3}$	1.9747
300	$5.15109 \cdot 10^{-4}$	1.9873	$4.89453 \cdot 10^{-4}$	1.9884
400	$2.90710 \cdot 10^{-4}$	1.9885	$2.76130 \cdot 10^{-4}$	1.9897
500	$1.86633 \cdot 10^{-4}$	1.9861	$1.77203 \cdot 10^{-4}$	1.9878

**Table 2** EOCs for the surface area preserving flow depicted in Fig. 3

$M$	$error_{max}$	EOC	$error_{L_1}$	EOC
<i>The surface <math>\mathcal{M}</math> with <math>\varphi(x, y) = x^2 - y^4</math></i>				
100	$3.7837 \cdot 10^{-4}$	–	$3.8695 \cdot 10^{-4}$	–
200	$9.4747 \cdot 10^{-5}$	1.9976	$9.6895 \cdot 10^{-5}$	1.9976
300	$4.2245 \cdot 10^{-5}$	1.9920	$4.3195 \cdot 10^{-5}$	1.9925
400	$2.3870 \cdot 10^{-5}$	1.9843	$2.4400 \cdot 10^{-5}$	1.9852
500	$1.5365 \cdot 10^{-5}$	1.9741	$1.5701 \cdot 10^{-5}$	1.9757
<i>The surface <math>\mathcal{M}</math> with <math>\varphi(x, y) = \sin(\pi y)</math></i>				
100	$4.82926 \cdot 10^{-3}$	–	$4.63840 \cdot 10^{-3}$	–
200	$1.23896 \cdot 10^{-3}$	1.9626	$1.19223 \cdot 10^{-3}$	1.9599
300	$5.51443 \cdot 10^{-4}$	1.9964	$5.30688 \cdot 10^{-4}$	1.9962
400	$3.10376 \cdot 10^{-4}$	1.9978	$2.98703 \cdot 10^{-4}$	1.9977
500	$1.98734 \cdot 10^{-4}$	1.9979	$1.91262 \cdot 10^{-4}$	1.9978

## 5 Conclusions

We studied the length and surface area preserving non-local geometric flows driven by the geodesic curvature and external force. We applied a projection method for a flow of surface curves into the underlying plane. We presented a formula for the normal velocity of a projected flow and we proposed a numerical discretization scheme. The scheme is based on the flowing finite volume method resulting in a semi-discrete scheme which can be solved by the method of lines. We presented results of computation of the length and surface area preserving flows. We also performed quantitative analysis of the experimental order of convergence of the numerical method showing the second order of convergence.

**Acknowledgements** Miroslav Kolář and Michal Beneš were partly supported by the project No. 14-36566G of the Czech Science Foundation and by the project No. OHK4-001/17 2017-19 of the Student Grant Agency of the Czech Technical University in Prague. The third author was supported by the VEGA grant 1/0062/18.

## References

1. M. Kolář, M. Beneš, D. Ševčovič, Area preserving geodesic curvature driven flow of closed curves on a surface. *Discrete Contin. Dyn. Syst. - Ser. B* **22**(10), 367–3689 (2017)
2. M. Kolář, M. Beneš, D. Ševčovič, Computational analysis of the conserved curvature driven flow for open curves in the plane. *Math. Comput. Simul.* **126**, 1–13 (2016)
3. I.C. Dolcetta, S.F. Vita, R. March, Area preserving curve shortening flows: from phase separation to image processing, *Interfaces Free Bound.* **4**, 325–343 (2002)
4. M. Gage, On an area-preserving evolution equation for plane curves. *Contemp. Math.* **51**, 51–62 (1986)
5. C. Kublik, S. Esedođlu, J.A. Fessler, Algorithms for area preserving flows. *SIAM J. Sci. Comput.* **33**, 2382–2401 (2011)

6. J. McCoy, The surface area preserving mean curvature flow. *Asian J. Math.* **7**, 7–30 (2003)
7. D. Ševčovič, S. Yazaki, On a gradient flow of plane curves minimizing the anisoperimetric ratio, *IAENG Int. J. Appl. Math.* **43**(3), 160–171 (2013)
8. J. Rubinstein, P. Sternberg, Nonlocal reaction-diffusion equations and nucleation. *IMA J. Appl. Math.* **48**, 249–264 (1992)
9. M. Beneš, S. Yazaki, M. Kimura, Computational studies of non-local anisotropic Allen-Cahn equation. *Math. Bohem.* **136**, 429–437 (2011)
10. J.W. Cahn, J.E. Hilliard, Free energy of a nonuniform system. III. Nucleation of a two-component incompressible fluid. *J. Chem. Phys.* **31**, 688–699 (1959)
11. S. Allen, J. Cahn, A microscopic theory for antiphase boundary motion and its application to antiphase domain coarsening. *Acta Metall.* **27**, 1085–1095 (1979)
12. I.V. Markov, *Crystal Growth for Beginners: Fundamentals of Nucleation, Crystal Growth, and Epitaxy*, 2nd edn. (World Scientific Publishing Company, Springer, 2004)
13. K. Deckelnick, Parametric mean curvature evolution with a Dirichlet boundary condition. *J. Reine Angew. Math.* **459**, 37–60 (1995)
14. K. Mikula, D. Ševčovič, Computational and qualitative aspects of evolution of curves driven by curvature and external force. *Comput. Vis. Sci.* **6**, 211–225 (2004)
15. K. Mikula, D. Ševčovič, A direct method for solving an anisotropic mean curvature flow of plane curves with an external force. *Math. Methods Appl. Sci.* **27**, 1545–1565 (2004)
16. D. Ševčovič, K. Mikula, Evolution of plane curves driven by a nonlinear function of curvature and anisotropy, *SIAM J. Appl. Math.* **61**, 1473–1501 (2001)
17. M. Beneš, J. Kratochvíl, J. Kříšťan, V. Minárik, P. Pauš, A parametric simulation method for discrete dislocation dynamics. *Eur. Phys. J. ST* **177**, 177–192 (2009)
18. M. Beneš, M. Kimura, P. Pauš, D. Ševčovič, T. Tsujikawa, S. Yazaki, Application of a curvature adjusted method in image segmentation. *Bull. Inst. Math. Acad. Sinica (N. S.)* **3**, 509–523 (2008)